JOURNAL OF AIRCRAFT
Vol. 49, No. 6, November–December 2012

Multibody Analysis of Terminal Phase for a Reentry Vehicle: A Comparative Study

Giulio Avanzini*
Università del Salento, 72100 Brindisi, Italy
and
Giorgio Guglieri† and Alberto Torasso‡
Politecnico di Torino, 10129 Turin, Italy

DOI: 10.2514/1.C031788

The multibody analysis of the system formed by an entry vehicle and a parachute is the subject of the present paper. In particular, two different models of the system made of bridles (connecting the vehicle to the suspension point) and riser (connecting the suspension point to the suspension lines of the parachute) are considered. This allows one to highlight if and how the simplifying assumptions at the basis of many techniques adopted for sizing the suspension system are reasonable and if they affect the most important factors that characterize the final phase of an entry trajectory, such as peak load and maximum deceleration at parachute inflation and landing site dispersion footprint. A Monte Carlo analysis is performed to account for uncertainties on initial conditions and system parameters.

Downloaded by Giorgio Guglieri on December 6, 2012 | http://arc.aiaa.org | DOI: 10.2514/1.C031788

Nomenclature

C_l, C_m, C_n	=	roll, pitch, and yaw moment coefficients
C_r	=	riser damping coefficient
C_X, C_Y, C_Z	=	axial, lateral, and normal force coefficient
D, Y, L	=	drag, lateral, and lift forces
D_P	=	parachute diameter
$\boldsymbol{f}_i$	=	bridles tension, $i = 1, 2, 3, 4$
$\boldsymbol{f}_r$	=	riser tension
g	=	acceleration of gravity
I_{ay}	=	parachute added mass moment of inertia
I_x, I_y, I_z, I_{xz}	=	mass moments of inertia
K_i	=	stiffness coefficient, $i = a, f, r$
L, M, N	=	roll, pitch, and yaw moments
ℓ_{ref}	=	reference length
M	=	Mach number
m	=	mass
m_{ax}, m_{ay}	=	axial and transverse added masses of the parachute
q_∞	=	dynamic pressure
S_P	=	parachute reference area
S_{ref}	=	vehicle reference area
V	=	airspeed
$\boldsymbol{v} = (u, v, w)^T$	=	velocity
W	=	weight
X, Y, Z	=	axial, lateral, and normal force
x, y, $-h$	=	longitudinal, cross-track, and vertical position in Earth-fixed axes
α, β	=	vehicle angle of attack and sideslip
γ	=	flight-path angle
ζ	=	nondimensional damping
λ, δ	=	riser azimuth and elevation angles
ρ	=	air density
$\boldsymbol{\rho}_i$	=	riser or bridle versor, $i = 1, \cdots, 4, r$
ϕ, θ, ψ	=	Euler angles
$\boldsymbol{\omega} = (p, q, r)^T$	=	angular velocity

Subscripts

A	=	bridles convergence point
a	=	aft bridles
B	=	parachute riser attach point
f	=	front bridles
P	=	parachute
r	=	riser
V	=	vehicle
0	=	reference condition

Received 14 December 2011; revision received 16 May 2012; accepted for publication 18 May 2012. Copyright © 2012 by the American Institute of Aeronautics and Astronautics, Inc. All rights reserved. Copies of this paper may be made for personal or internal use, on condition that the copier pay the $10.00 per-copy fee to the Copyright Clearance Center, Inc., 222 Rosewood Drive, Danvers, MA 01923; include the code 0021-8669/12 and $10.00 in correspondence with the CCC.

*Professor, Department of Engineering, Edificio 14 Cittadella della Ricerca, SS 7 Km.7.3. Senior Member AIAA.

†Associate Professor, Department of Mechanical and Aerospace Engineering, Corso Duca degli Abruzzi 24. Senior Member AIAA.

‡Ph.D. Candidate, Department of Mechanical and Aerospace Engineering, Corso Duca degli Abruzzi 24. Member AIAA.

I. Introduction

UNLESS a gliding vehicle is considered, which lands like a conventional airplane, the terminal phase of a planetary entry trajectory is performed by completing the deceleration before touchdown (or splashdown) by means of a passive aerodynamic deceleration system. This system is made by a sequence of drogue and main parachute (or cluster of parachutes). The former decelerates the vehicle from mild supersonic or transonic speed, whereas the latter completes the deceleration from low speed to the final touch- or splashdown speed. During parachute inflation, high loads are transmitted by the suspension system to the vehicle. The determination of peak loads, peak values of tension in the elements of the suspension system, the deceleration profile, and the landing footprint are all aspects relevant to the design of an aerodynamic deceleration system. This paper deals with the analysis of two possible multibody models for the description of the system formed by a parachute and a lifting-body reentry vehicle, during the whole terminal phase, from inflation of the first parachute in the sequence to touchdown.

An intense research activity concerning reentry configurations (planetary entry probes and manned capsules) and the analysis of their decelerated reentry phase was performed during the early development of space missions. More recently, a renewed interest on the subject emerged, as new European research programs [such as Atmospheric Reentry Demonstrator (ARD), Expert, Intermediate Experimental Vehicle (IXV), ExoMars, and Advanced Reentry Vehicle] concerning capsule aerodynamics and flight dynamics have been either started or carried out. Two relevant examples are the

Downloaded by Giorgio Guglieri on December 6, 2012 | http://arc.aiaa.org | DOI: 10.2514/1.C031788

Atmospheric Reentry Demonstrator and the Intermediate Experimental Vehicle.

The ARD was a technology demonstrator [1–3] that has been developed by the European Space Agency. The design of the ARD was based on the geometry of the Apollo Command Module and it was substantially a scaled version of the original Apollo capsule. The complete ARD mission was successfully performed after the Ariane 503 flight in 1998. Attitude dynamics of the Atmospheric Reentry Demonstrator during parachute deployment and final deceleration phase was analyzed by means of multibody dynamics [1]. The simulation of parachute inflation and descent phase was compared with flight test data. Parachute loads and payload accelerations were correctly predicted, whereas some discrepancies were observed for attitude dynamics that are substantially affected by gusts and atmospheric turbulence. The accuracy of attitude simulations was also influenced by the uncertainty of available aerodynamic data for the damping coefficients of the capsule [4]. Static and oscillatory data were measured for a reference model of Apollo Command Module (ACM) [5] to extend the available experimental database to different test conditions. An extended higher order mathematical model was validated by comparing the results of simulations with flight test data for the terminal reentry phase of the ARD mission [6].

The IXV project is the next core step of the European experimentation effort. The IXV project [7,8] builds on previous European achievements in the framework of space transportation systems and technologies, and it will bring significant advancements with respect to previous European flying test beds. IXV uses a lifting body configuration with no wings or stabilizing surfaces, using two movable flaps for reentry flight control. The IXV key mission and system objectives are the design, development, manufacturing, assembly, and on-ground to in-flight verification of an autonomous European lifting and aerodynamically controlled reentry system, integrating the critical reentry technologies at a system level. Among such critical technologies of interest, special attention is paid to advanced instrumentation for aerodynamics and aerothermodynamics, various thermal protections and hot structures solutions, guidance, navigation, and flight control through combined jets, aerodynamic flaps, and decelerators.

Both ARD and IXV missions end with a terminal reentry phase, in which the final deceleration is controlled by a sequence of parachutes. This feature revitalizes the interest for the availability, during the design phase, of numerically efficient, yet comprehensive simulation models of body-parachute systems, which allow statistical and/or parametric analyses of mission profiles, including the effects of uncertainties and an adequate level of dynamic coupling to reliably assess overall system stability and performance parameters (such as peak deceleration factors, maximum tension in the suspension system, etc.).

Several studies [9–14] analyze the entry, descent, and landing trajectories of returning capsules. These analyses consist of performing a simulation of the atmospheric entry phase to predict deceleration peaks, descent attitudes, and terminal conditions. A 6 DOF rigid-body model is typically adopted. In addition, a stochastic dispersion analysis (Monte Carlo or similar) is often performed to assess the impact of off-nominal conditions that may arise during the entry to determine the robustness of the mission design. Specifically, the attitude of the reentry vehicle near parachute deployments is of interest, along with the landing or splashdown footprints. Note that the dynamic stability of blunt bodies like capsules and planetary entry probes has been shown to be poor in subsonic flight [15]. The near-wake recirculation and the rear flowfield pattern are responsible for the unstable dynamic behavior as a consequence of time lags in the wake [16].

The deceleration required to control the airspeed of the capsule during the terminal phase of the reentry may be provided by means of parachutes [17,18]. A complete overview of parachute technology including aerodynamics and payload-decelerator dynamics is given in [19,20]. An introduction to the development and application of aerodynamic decelerators for robotic planetary exploration missions is given in [21]. For many applications, parachute and capsule systems can be treated as a single rigid body. This method is sufficient when only the trajectory of the payload must be simulated. Two coupled bodies must be considered when the relative motion of the two subsystems is of interest for a complete simulation of attitude dynamics and the determination of peak loads in the suspension system during parachute deployment.

A two-dimensional parachute model is presented in [22] to compute various characteristics of the steady descent of a parachute system. A 3 degree-of-freedom analysis is presented and validated in [23], where the longitudinal motion of a typical vehicle during the recovery phase is presented. The parachute and the payload are supposed to be rigid and interconnected by an elastic riser. Aerodynamic loads acting on the two subsystems are considered. Computer results showed good agreement with test results in terms of oscillation amplitude and frequency, riser force, and parachute wrap up about the vehicle for the simulation of a pad-abort situation.

The three-dimensional motion of a freely descending parachute is studied in [24] with a 5 degree-of-freedom analysis (roll motion is neglected). Exact expressions are given for the longitudinal and lateral small disturbance stability of the gliding motion of parachutes. The analysis confirms that large longitudinal disturbance of most parachutes will result in a large pitching motion, whereas a large lateral disturbance will usually cause a large angle vertical coning motion (coning mode). The longitudinal mode damps out very quickly in the stable case.

The three-dimensional motion of a nonrigid parachute and payload system is studied in [25]. Both the parachute and the payload are assumed to have 5 degrees of freedom (roll about axis of symmetry is again neglected). They are coupled together by a fixed-length connector. The general nonlinear equations are linearized using small perturbation theory. The evaluation of the stability of an unstable payload decelerated by a parachute is performed. The authors observed that increasing riser length and parachute weight promotes system instability.

A 9 degree-of-freedom computer program was developed in [26] for the simulation of the trajectory and the dynamic behavior of a rotating parachute system. An accurate mathematical model of the joint between the load and the parachute was found to be necessary to predict the dynamic behavior of a rotating decelerated system.

A computer model based on a 6 degree-of-freedom analysis is described in [27] and compared with drop test data. The payload is rigidly connected, the aerodynamic forces on canopy and payload are determined by the instantaneous angle of attack of the impinging airflow, and the apparent masses are constant, but they depend on the direction of the acceleration.

Full nonlinear equations of motion for the axisymmetric parachute have been obtained in [28]. In particular, the correct form of the added mass tensor for a rigid axisymmetric parachute in ideal flow was implemented in a 6 degree-of-freedom computer model [29] and the results indicate that added mass effects are significant. In particular, the component of added mass along the axis of symmetry has a strong effect on parachute dynamic stability. However, design and testing experience proved that dynamic stability of the parachute is a second-order design problem [20] for high-performance decelerators, which usually have both high static and dynamic stability due to the porosity of the canopy.

It is clear that one of the most crucial issues when dealing with multibody models of the system, formed by parachute and vehicle connected by suspension lines, is the representation of actions exchanged between the two bodies through the suspension system. In general, a suspension system is made by a set of bridles (usually two for capsules, three or four for lifting bodies) that connect the vehicle to the riser which, in turn, connects the suspension point A, where the bridles converge to the point B, where the suspension lines of the parachute converge, as depicted in Fig. 1.

It is common practice to assume that the assembly of parachute and suspension lines can be considered as rigid. Options are different for the riser and the bridles. Many works, including more recent models developed and validated by means of drop tests, consider the bridles as rigid [30,31]. In this case, the only elastic element in the whole suspension system is the riser. This greatly simplifies the analysis, especially for a two-dimensional study, because the position of A

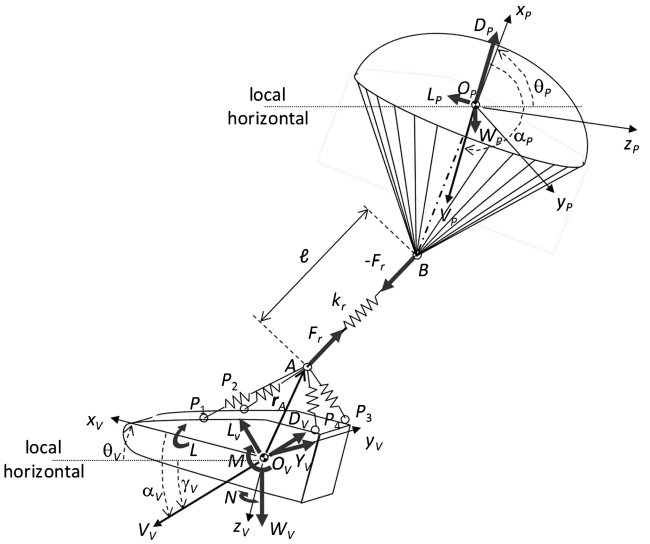

Fig. 1 Sketch of the multibody system (vehicle, bridles, riser, and parachute).

becomes known for nominal conditions in which the riser lies within the angle identified by the bridles, or it is easily derived from simple geometric considerations, if the riser lies outside of this angle. Things change when a three-dimensional picture of the trajectory is required (e.g., if lateral displacement of the center of gravity of the vehicle need to be included in the analysis, which may result in the bridles on one side of the vehicle to be more loaded than the other ones) or when four bridles are used, which prevents the determination of tension in the bridles from a mere projection of riser force along their direction.

In this case, the simulation of the full-order model of decelerated reentry vehicles becomes complex. A first simplified approach can be based on decoupling longitudinal- and lateral-directional dynamics, resulting in two-dimensional (or planar) models. These reduced-order models correctly reproduce the most relevant features of the trajectory of the suspended body, at the cost of neglecting inertial couplings between orthogonal axes, typical of rotary dynamics (pitch, yaw, and roll response). A three-dimensional model, characterized by a reasonably accurate representation of the suspension system, overcomes these limits, improving the reliability of the representation of vehicle attitude dynamics and the estimate of tensions in bridles and riser. This complexity, far from being a mere cosmetic added value, if neglected, may preclude the prediction of off-nominal in-flight behaviors of the suspension system, quite frequently observed during these types of missions.

The objectives of the present study are 1) to derive two three-dimensional models of the suspension system, one where the bridles are assumed as inextensible, and a second one, where bridle elasticity is included; 2) to analyze if the assumptions of an inextensible set of bridles provides an advantage in terms of computational efficiency; and 3) to verify if this assumption provides a reliable estimate of peak loads on vehicle and suspension system, while keeping tension values within reasonable limits. The determination of peak loads is performed by means of a Monte Carlo analysis, in which the effects of different initial and parachute release conditions are evaluated.

In what follows, the next section of the paper describes in detail the geometry of the system and the mathematical models developed for vehicle and parachute dynamics. In Sec. III, a semi-analytical solution for the determination of bridle tension is developed, assuming bridles as inextensible. This model is compared with a numerical one, where bridles are considered as elastic cables. In the Sec. IV, after describing the nominal solution for the parachute sequence assumed for the study, a Monte Carlo analysis is performed to identify if and how the bridle model has an impact on the identification of critical system parameters and/or computational performance. A section of concluding remarks ends the paper.

II. Vehicle and Parachute Mathematical Models

A. Modeling Approach

Figure 1 depicts the scheme of the system studied, made by a rigid vehicle, a parachute, and the suspension system. The latter is formed by four bridles that connect four attach points on the vehicle with a riser. The riser, in turn, connects the bridles to the suspension lines attached to the canopy of the parachute. The parachute with its suspension lines is modeled as a rigid body.

The riser is always assumed as an elastic cable, whereas two different models are considered for the bridles. In one case, they are assumed as inextensible, so that their length is constant and the position of the attach point A with the riser is known and prescribed most of the times, unless the riser swings longitudinally or laterally and pulls the bridles on one side only, loosening two or three of them. In this case, a search is to be performed to identify the position of A on the basis of some geometrical considerations. The assumption of inextensible bridles is quite common [30], but to investigate its consequences on the determination of tension and deceleration peak values, a model that features elastic bridles is also developed, in which case the position of the attach point A needs to be searched iteratively.

The deceleration takes place in a standard atmosphere with no winds. The analysis of the effects of winds on the landing footprint is out of the scopes of the present work. Gravity acceleration g is assumed constant and vehicle and parachute motion is analyzed, neglecting the effects of Earth's rotation and curvature, which are reasonable assumptions for the velocity and altitude ranges considered. The main features of the models for the three elements of the system are reported in what follows. Reference to the relevant literature is provided for details omitted here for the sake of conciseness.

B. Vehicle Model

The fictitious vehicle considered in the test cases is a lifting body with a configuration similar that described in [7,8]. Relevant data for the vehicle are reported in the first portion of Table 1. Expressing vector components in a set of body axes $\mathcal{F}_V$, the equations of motion are written in compact form as

$$\begin{aligned}
\dot{\boldsymbol{v}}_V + \boldsymbol{\omega}_V \times \boldsymbol{v}_V &= (\boldsymbol{f}_{A_V} + \boldsymbol{f}_{r_V})/m + \boldsymbol{g}_V \\
\boldsymbol{I}\dot{\boldsymbol{\omega}}_V + \boldsymbol{\omega}_V \times (\boldsymbol{I}\boldsymbol{\omega}_V) &= \boldsymbol{m}_{A_V} + \boldsymbol{r}_{A_V} \times \boldsymbol{f}_{r_V} \\
\dot{\boldsymbol{\Phi}} &= \mathbb{R}(\theta, \phi)\boldsymbol{\omega}_V \\
\dot{\boldsymbol{r}}_I &= \mathbb{T}_{IV}(\phi, \theta, \psi)\boldsymbol{v}_V
\end{aligned} \tag{1}$$

where $\boldsymbol{f}_{A_V}$ and $\boldsymbol{m}_{A_V}$ are aerodynamic force and moment, respectively, $\boldsymbol{f}_{r_V}$ represents riser tension, whereas the expression of gravity acceleration in the body frame is given by $\boldsymbol{g}_V = g(-\sin\theta, \cos\theta\sin\phi, \cos\theta\cos\phi)^T$, with $g = 9.81\ \mathrm{m/s^2}$ assumed constant. The state variables are vehicle velocity components $\boldsymbol{v}_V = (u, v, w)^T$, its angular speed $\boldsymbol{\omega}_V = (p, q, r)^T$, roll, pitch, and yaw angles $\boldsymbol{\Phi} = (\phi, \theta, \psi)^T$, and, finally, the position of the vehicle center of mass $\boldsymbol{r}_I = (x, y, -h)^T$.

Letting $s\alpha = \sin(\alpha)$ and $c\alpha = \cos(\alpha)$, the expressions for the coordinate transformation matrix $\mathbb{T}_{IV}$ and the Euler angle rate matrix $\mathbb{R}(\theta, \phi)$ are given, respectively, by [32]

$$\mathbb{T}_{IV}(\phi, \theta, \psi) = \begin{bmatrix} c\theta c\psi & s\phi s\theta c\psi - c\phi s\psi & c\phi s\theta c\psi + s\phi s\psi \\ c\theta s\psi & s\phi s\theta s\psi + c\phi c\psi & c\phi s\theta s\psi - s\phi c\psi \\ -s\theta & s\phi c\theta & c\phi c\theta \end{bmatrix}$$

and

$$\mathbb{R}(\theta, \phi) = \begin{bmatrix} 1 & s\phi s\theta/c\theta & \cos\phi s\theta/c\theta \\ 0 & c\phi & -s\phi \\ 0 & s\phi/c\theta & c\phi/c\theta \end{bmatrix}$$

Aerodynamic forces and moments are expressed as

$$\boldsymbol{f}_{A_V} = \frac{1}{2}\rho(h) S_{\mathrm{ref}} V^2 (C_X, C_Y, C_Z)$$

$$\boldsymbol{m}_{A_V} = \frac{1}{2}\rho(h) S_{\mathrm{ref}} V^2 \ell_{\mathrm{ref}} (C_\ell, C_m, C_n)$$

where aerodynamic coefficients are given by

Downloaded by Giorgio Guglieri on December 6, 2012 | http://arc.aiaa.org | DOI: 10.2514/1.C031788

Table 1 Vehicle and parachute data

Parameter	Symbol	Value	Units
	Vehicle		
Mass	m	2000	kg
Reference area	S_{ref}	7.5	m^2
Reference length	ℓ_{ref}	4.5	m
Bridles attach points in $\mathcal{F}_V$: front	$\boldsymbol{r}_{P_{1,2}}$	$[0.4, \mp 0.4, -0.5]^T$	m
aft	$\boldsymbol{r}_{P_{3,4}}$	$[-1.7, \pm 0.4, -0.5]^T$	m
	Drogue		
Nominal diameter	D_P	5.00	m
Length of canopy suspension lines	ℓ_S	7.5	m
Riser unstretched length	ℓ_{r_0}	9	m
Front bridle unstretched length	ℓ_{f_0}	5.5	m
Aft bridle unstretched length	ℓ_{a_0}	4.0	m
Stiffness (spring constant)	K_r	170	kN/m
Damping coefficient	ζ_r	0.02	
	Main parachute		
Nominal diameter	D_P	33.00	m
Length of canopy suspension lines	ℓ_S	35	m
Riser unstretched length	ℓ_{r_0}	4.5	m
Front bridle unstretched length	ℓ_{f_0}	4.7	m
Aft bridle unstretched length	ℓ_{a_0}	4.5	m
Stiffness (spring constant)	K_r	170	kN/m
Damping coefficient	ζ_r	0.02	
Reefing (partial inflation for 10 s)		7	%

$$C_i = C_{i,0}(\alpha) + \Delta C_i(M) + C_{i_q}\hat{q} \quad \text{for } i = X, Z, m$$

$$C_i = C_{i,0}(\alpha) + \Delta C_i(M) + C_{i_\beta}\beta + C_{i_p}\hat{p} + C_{i_r}\hat{r} \quad \text{for } i = Y, \ell, n$$

where $V = (u^2 + v^2 + w^2)$ and $\hat{x} = x\ell_{\text{ref}}/(2V)$, with $x = p$, q, or r. The baseline term $C_{i,0}(\alpha)$ is obtained by linear interpolation of coefficients provided at various angles of attack α. The final phase of the deceleration is started at high subsonic speed, so that a correction $\Delta C_i(M)$ to the baseline term is required for $M > 0.5$. Note that longitudinal- and lateral-directional aerodynamic coefficients are decoupled and that the effects of sideslip angle and angular velocity components are represented by means of linear increments, which provide an acceptable estimate of aerodynamic coefficients only for small values of β, $\hat{p}$, $\hat{q}$, and $\hat{r}$. Simulations demonstrate that no high spin rate nor large sideslip angle build up during the final phase of the deceleration, so that these assumptions are reasonable at least for the vehicle here considered, which proved to be directionally stable.

C. Parachute

The parachute is modeled as a rigid body in the fully inflated configuration, neglecting deformations in the canopy (assumed as axisymmetric) and elasticity of the suspension lines. Data for drogue and main parachute are reported in Table 1, together with the characteristics of the suspension system. The equations of motion for the parachute [28,29] are expressed in a set of body axes $\mathcal{F}_P$, where x_P points along the axis of symmetry of the canopy. These equations are different from those for a conventional rigid body because the inertial terms include the contribution of added masses:

$$\begin{aligned}
(m_P\mathbf{1}_3 + \boldsymbol{M}_a)(\dot{\boldsymbol{v}}_P + \boldsymbol{\omega}_P \times \boldsymbol{v}_P) &= \boldsymbol{f}_{A_P} - \boldsymbol{f}_{r_P} + m_P\boldsymbol{g}_P \\
(\boldsymbol{I} + \boldsymbol{I}_a)\dot{\boldsymbol{\omega}}_P + \boldsymbol{v}_P \times \boldsymbol{M}_a\boldsymbol{v}_P + \boldsymbol{\omega}_P \times [(\boldsymbol{I} + \boldsymbol{I}_a)\boldsymbol{\omega}_P] &= \boldsymbol{m}_{A_P} - \boldsymbol{r}_{B_P} \times \boldsymbol{f}_{r_P} \\
\dot{\boldsymbol{\Phi}}_P &= \mathbb{R}(\theta_P, \phi_P)\boldsymbol{\omega}_P \\
\dot{\boldsymbol{r}}_P &= \mathbb{T}_{IP}(\phi_P, \theta_P, \psi_P)\boldsymbol{v}_P
\end{aligned} \tag{2}$$

where m_P and $\boldsymbol{I} = \text{diag}(I_{x_P}, I_{y_P}, I_{y_P})$ are mass and inertia tensor of the parachute, respectively, whereas $\mathbf{1}_3$ is the 3×3 identity matrix. Added mass are represented by the matrices $\boldsymbol{M}_a = \text{diag}(m_{a_x}, m_{a_y}, m_{a_y})$ and $\boldsymbol{I}_a = \text{diag}(0, I_{a_y}, I_{a_y})$, where m_{a_x} and m_{a_y} are axial and transverse added masses, and I_{a_y} is the added transverse moment of inertia. No added moment of inertia is present around the axis of the canopy. Note that, given a riser tension $\boldsymbol{f}_r$ applied at point A on the vehicle side, the tension acting on the parachute, applied at point B, is equal to $-\boldsymbol{f}_r$. The matrices $\mathbb{R}(\theta_P, \phi_P)$ and $\mathbb{T}_{IP}(\phi_P, \theta_P, \psi_P)$ in the kinematic equations for parachute attitude angles $\boldsymbol{\Phi}_P = (\phi_P, \theta_P, \psi_P)^T$ and position $\boldsymbol{r}_P = (x_P, y_P, -h_P)^T$ are defined in the same way as those used for the equations of motion of the vehicle.

Added masses m_{a_x}, m_{a_y}, and I_{a_y} are computed with the method adopted in [27], based on the use of multipliers of the mass of air included by the canopy scaled to match the effects of porosity. Because of the symmetry of the canopy, the transverse added mass m_{a_y} and inertia I_{a_y} are not influenced by the selection of the direction of the lateral axis y_P. The term I_{xz_P} is dropped in the moment equations, assuming that the body axes are also the principal axes of the parachute and that the center of parachute apparent mass is coincident with parachute center of mass.

The main aerodynamic load acting on the parachute is drag $D_P = q_\infty C_{DP} S_P$, which is aligned with the local direction of airspeed $\boldsymbol{v}_P$. A certain amount of lift L_P is also present. Both lift and drag forces vary with canopy angle of attack. Aerodynamic damping of the canopy is estimated according to the analytical method described in [33]. An efficiency factor for body wake interaction is introduced as a multiplier of dynamic pressure at canopy for the parachute. Inflation is modeled by ramping the value of drag area, given by the product of drag coefficient and projected area. The effective drag area is time scheduled according to the planned reefing stages and inflation times. The instantaneous added mass and inertia tensor are calculated on the basis of the effective drag area and local air density.

III. Suspension System

The suspension systems used for drogue and main parachute have the same layout: Four bridles and a riser connect the vehicle to the suspension lines of the canopy. The bridles are attached to suspension points on the vehicle, labeled P_i, $i = 1, 2, 3, 4$ in Fig. 1. The bridles are connected to a riser at point A, whereas the canopy suspension lines converge at point B, at the other end of the riser. The position of B in the parachute frame $\mathcal{F}_P$ is fixed, whereas the position of A in the vehicle body frame $\mathcal{F}_V$, in general, is not. The determination of A in $\mathcal{F}_V$ marks the most significant difference between the two models compared in this work, that is, the model featuring inextensible bridles and the fully elastic model, where both riser and bridles stretch under the action of the tension in the suspension system.

Downloaded by Giorgio Guglieri on December 6, 2012 | http://arc.aiaa.org | DOI: 10.2514/1.C031788

Downloaded by Giorgio Guglieri on December 6, 2012 | http://arc.aiaa.org | DOI: 10.2514/1.C031788

A. Inextensible Bridles

In many studies, the only elastic element in the suspension system is the riser [30]. The tension force exchanged between parachute and vehicle is thus easily derived, once the position of the attach points of the riser A and B, on vehicle and parachute side, respectively, are determined in the same frame (e.g., in the fixed frame $\mathcal{F}_I$). The tension is proportional to the elongation of the riser and it acts in the direction connecting A to B. Given the state vector for the parachute, the position of the riser suspension point B on the parachute side is known because of the assumption of a rigid assembly for canopy and suspension lines. The position of B in the inertial frame is given by

$$\boldsymbol{r}_{B_I} = \boldsymbol{r}_P + \mathbb{T}_{IP}\boldsymbol{r}_{B_P}$$

where $\boldsymbol{r}_{B_P} = (-\ell_B, 0, 0)^T$ is the (fixed) position of the attach point B in $\mathcal{F}_P$.

On the converse, even when a fixed length for the bridles is assumed, the riser attach point A on the vehicle's side is not in a fixed position in the body frame. Its nominal position A_0 is identified in $\mathcal{F}_V$ by the position vector $\boldsymbol{r}_{A_{0,V}}$, such that the distance of A_0 from the attach points P_i, $i = 1, 2, 3, 4$ is equal to the length of the bridles. This is equivalent to the conditions $\|\boldsymbol{r}_{A_{0,V}} - \boldsymbol{r}_{P_{1,2}}\| = \ell_f$ and $\|\boldsymbol{r}_{A_{0,V}} - \boldsymbol{r}_{P_{3,4}}\| = \ell_a$, where ℓ_f and ℓ_a are the lengths of forward and aft bridles, respectively.

Point A lies in A_0 only, provided that the direction of riser tension falls within the solid angle limited by the faces of the prolongation of bridles beyond A_0. When the parachute swings either longitudinally or laterally, as it happens during the initial deployment phase, the direction of the riser may fall outside of the solid angle defined by the bridles. Provided that peak values of vehicle deceleration and tension in the suspension system are reached during this critical phase, it is clearly important to correctly evaluate how the attach point A moves under the action of the forces exchanged between riser and bridles, to provide reliable estimates of deceleration force transmitted to the vehicle and peak values of the tension reached in each element of the suspension system for correctly sizing it against worst case scenarios.

1. Longitudinal Case

For a purely longitudinal model, the simple approach proposed in [30] is sufficient, and its implementation can be summarized as follows, with reference to the sketch drawn in Fig. 2. Points P_f and P_a lie on the longitudinal plane, between the forward (P_1 and P_2) and the aft (P_3 and P_4) attach points of the bridles, respectively. If the direction of the riser falls within the angle $\widehat{P_f A_0 P_a}$, as in Fig. 2a (case 0), the attach point A of the riser lies in its nominal position A_0. Tension in the riser $\boldsymbol{f}_r$ is projected along the directions of segments $\overline{P_f A_0}$ and $\overline{P_a A_0}$, such that the sum $\boldsymbol{f}_a + \boldsymbol{f}_f + \boldsymbol{f}_r = 0$. Tension in each bridle is finally determined from symmetry considerations, such that $\boldsymbol{f}_1 + \boldsymbol{f}_2 = \boldsymbol{f}_f$ and $\boldsymbol{f}_3 + \boldsymbol{f}_4 = \boldsymbol{f}_a$.

If, on the converse, the riser lies outside of the angle $\widehat{P_f A_0 P_a}$, one pair of bridles loses tension: If the riser is pulling backward (as shown in Fig. 2b), case 1 is dealt with, where the aft pair of bridles loses tension, whereas the forward pair is not taut in case 2, when the riser pulls forward of the direction of the segment $\overline{P_a A_0}$. In case 1, letting $\bar{\ell}_f$ be the length of the projections of forward bridles on the longitudinal plane, A lies at the intersection of a circle of radius $\bar{\ell}_f$ centered in P_f with the line connecting P_f to B. This point is easily determined analytically, once the position of B is projected in the vehicle's body frame $\mathcal{F}_V$. Similarly, for case 2 (not reported in the figures), point A lies at the intersection of a circle of radius $\bar{\ell}_a$ centered in P_a with the line connecting P_a to B. In both cases, the tension in the riser is transmitted only to the bridles in tension.

2. Three-Dimensional Case

When a three-dimensional motion is considered, point A can still be determined analytically, but a less trivial search algorithm is required because the set of possible positions for point A and the determination of the configuration for the bridles in tension at each time follows a more complex pattern. As stated earlier, the four bridles are simultaneously in tension (case 0) only if the riser lies within the solid angle inside the prolongations of the segments connecting A_0 with the attach points P_i, $i = 1, 2, 3, 4$. This condition is determined analytically in what follows.

Initially, one assumes that $A \equiv A_0$. Given the nominal position $\boldsymbol{r}_{A_{0,V}} = (x_{A,0}, 0, z_{A,0})^T$ of A in $\mathcal{F}_V$ for the considered system geometry, its inertial position is expressed as

$$\boldsymbol{r}_{A_I} = \boldsymbol{r}_I + \mathbb{T}_{IV}\boldsymbol{r}_{A_{0,V}}$$

It is then possible to determine the length of the riser $\ell_r = \|\boldsymbol{r}_{A_I} - \boldsymbol{r}_{B_I}\|$. The tensions exchanged between vehicle and parachute are expressed as $\boldsymbol{f}_{r_I} = F_r(\boldsymbol{r}_{A_I} - \boldsymbol{r}_{B_I})/\ell_r$, with

$$F_r = K_r(\ell_r - \ell_{r_0}) - C_r\dot{\ell}_r \quad \text{if } \ell_r > \ell_{r_0} \qquad F_r = 0 \quad \text{if } \ell_r < \ell_{r_0}$$

Let $\hat{\boldsymbol{\rho}}_i = (x_i, y_i, z_i)^T$, $i = 1, 2, 3, 4$, be the unit vectors aligned with the segments $\overline{P_i A_0}$, and $\hat{\boldsymbol{\rho}}_r = (x_r, y_r, z_r)^T$ the unit vector parallel to the tentative direction of the riser $\overline{A_0 B}$, whereas Π is a plane perpendicular to the direction of the z_V body axes at a distance d above A_0. The coordinates of points Q_i at the intersection of the prolongation of the ith bridle with plane Π are given by $(x_{A,0}, 0, z_{A,0})^T + (d/z_i)(x_i, y_i, z_i)^T$, whereas point R at the intersection of the riser with Π is given by $(x_{A,0}, 0, z_{A,0})^T + (d/z_r)(x_r, y_r, z_r)^T$. In the most general case, points Q_i identify a trapezoid on Π, such that $x_1 = x_2 = x_f$ and $x_3 = x_4 = x_a$. For symmetry reasons, one usually has $y_1 = -y_2$ and $y_4 = -y_3$, but, in general $y_2 = y_f \neq y_3 = y_a$. The riser lies inside the solid angle defined by the bridles if the following inequalities are satisfied:

$$x_a \leq x_r \leq x_f; \qquad -y_{\lim}(x_r) \leq y_r \leq y_{\lim}(x_r) \tag{3}$$

with $y_{\lim}(x_r) = y_a + (y_f - y_a)(x_r - x_a)/(x_f - x_a)$. The violation of any one of the limits reported in Eq. (3) means that the riser is outside of the solid angle and at least two bridles lose tension.

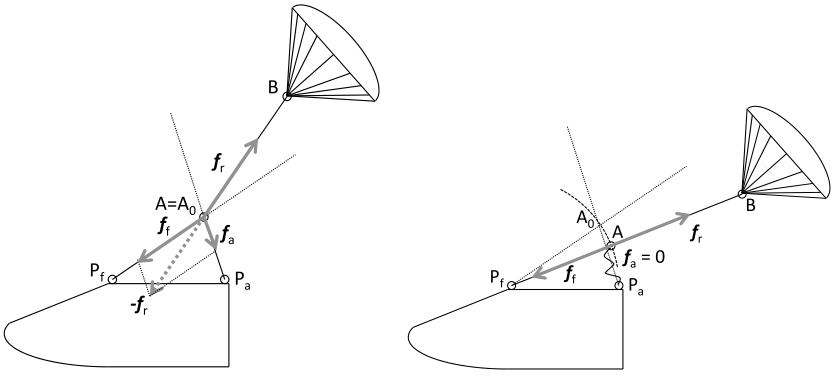

Fig. 2 Position of riser attach point A for inextensible bridles in longitudinal case: a) forward and aft bridles loaded; b) load on front bridles only.

Downloaded by Giorgio Guglieri on December 6, 2012 | http://arc.aiaa.org | DOI: 10.2514/1.C031788

If the inequalities in Eq. (3) are satisfied, the tension in the bridles must satisfy the equation

$$\sum_{i=1}^{4} f_i \hat{\boldsymbol{\rho}}_i + \boldsymbol{f}_r = 0 \tag{4}$$

Equation (4) can be recast in matrix form, $\boldsymbol{R}\boldsymbol{\phi} = \hat{\boldsymbol{f}}_r$, where the 3×4 matrix $\boldsymbol{R}$ is defined as $\boldsymbol{R} = [\hat{\boldsymbol{\rho}}_1 \vdots \hat{\boldsymbol{\rho}}_2 \vdots \hat{\boldsymbol{\rho}}_3 \vdots \hat{\boldsymbol{\rho}}_4]$. Assuming that tension in the bridles minimizes the sum of the strain energy in each bridle, proportional to its tension, the coefficients $\boldsymbol{\phi} = (f_1, f_2, f_3, f_4)^T$ can be obtained by means of the Moore–Penrose pseudoinverse $\boldsymbol{R}^* = \boldsymbol{R}^T(\boldsymbol{R}\boldsymbol{R})^{-1}$, which provides the minimum-norm solution to Eq. (4). One thus obtains for the tension the expression $(f_1, f_2, f_3, f_4)^T = \boldsymbol{R}^T(\boldsymbol{R}\boldsymbol{R})^{-1}\boldsymbol{f}_r$. Note that the Moore–Penrose pseudoinverse matrix needs to be evaluated only once, for the considered geometry of the bridles.

At this point, it is possible to accept the solution for the tension in the suspension system if and only if all the bridles are in tension, that is, all the f_i are positive. If the tension in the jth bridle turns negative, that bridle should provide a compression force, which is clearly unfeasible. This may happen at points close to the boundaries of case 0. Assuming that $f_j = 0$, the tension in the remaining three bridles is obtained by solving the linear system

$$\sum_{\substack{i=1 \\ i \neq j}}^{4} f_i \hat{\boldsymbol{\rho}}_i + \boldsymbol{f}_r = 0 \tag{5}$$

where a 3×3 matrix obtained from the unit vectors $\hat{\boldsymbol{\rho}}_i$, $i \neq j$ can be easily analytically inverted.

When the riser falls outside of the nominal solid angle, the tension of at least two bridles becomes negative, if derived with the procedure outlined earlier. When this happens, eight different cases are present, in which two or three bridles become loose, depending on the direction in which the riser is pulling, as shown qualitatively in Fig. 3. One pair of bridles is in tension and two are loose, when the riser swings mainly in the longitudinal direction with minor deviations from the longitudinal plane, or if it swings laterally, with just a minor longitudinal displacement. Four cases are possible, numbered with even numbers, where either the aft (case 2), forward (case 6), left (case 4), or right (case 8) pair of bridles are taut. In these cases, the bridles in tension and the riser lie on the same plane and the attach point A moves along arcs of a circle, as depicted in Fig. 4a.

As an example, consider case 6, in which only the forward pair of bridles are in tension. In this case, the two taut bridles and the riser must lie on the same plane Γ, which is identified from the positions of points P_1, P_2, and B. Let $\hat{\boldsymbol{\rho}}_{12}$ be the unit vector along the segment $\overline{P_1P_2}$ and $\hat{\boldsymbol{\rho}}_{1B}$ the unit vector parallel to the segment from P_1 to B. The normal to Γ is given by $\hat{\boldsymbol{n}}_\Gamma = (\hat{\boldsymbol{\rho}}_{12} \times \hat{\boldsymbol{\rho}}_B)/\|\hat{\boldsymbol{\rho}}_{12} \times \hat{\boldsymbol{\rho}}_B\|$. Point A lies along the direction identified by the unit vector $\hat{\boldsymbol{\gamma}} = (\gamma_x, 0, \gamma_z)^T = \hat{\boldsymbol{n}}_\Gamma \times \hat{\boldsymbol{\rho}}_{12}$, at a distance $\bar{\ell}_f$ from point P_a, that is, the coordinates of A are given by

$$(x_A, y_A, z_A)^T = (x_f, 0, z_f)^T + \bar{\ell}_f(x_\gamma, 0, z_\gamma)^T$$

In this case, point A lies on a circular arc on the longitudinal plane centered in P_a. Similar derivations can be obtained for all the other cases with two bridles in tension. For lateral motion of the riser, the two arcs of admissible positions for A lie on a plane perpendicular to the longitudinal plane of the vehicle.

If the riser moves both laterally and longitudinally, it may happen that three bridles lose tension at the same time and the only remaining bridle in tension aligns itself with the riser. Four more cases are thus present, numbered with odd numbers 1, 3, 5, and 7, such that only bridle number 3, 4, 1, or 2, respectively, is in tension. In this case A lies on a portion of a sphere, centered in the attach point of the only bridle in tension left (Fig. 4a). The position of A is now easily determined from the direction of the unit vector $\hat{\boldsymbol{\rho}}_{iB} = (x_{iB}, y_{iB}, z_{iB})^T$, parallel to the segment that connects P_i to B, where P_i is the attach point of the only bridle in tension. The position of A is thus given by

$$(x_A, y_A, z_A)^T = (x_i, y_i, z_i)^T + \ell_i(x_{iB}, y_{iB}, z_{iB})^T$$

The scheme depicted in Fig. 3 represents the position of the riser with respect to the pyramid in the various cases only qualitatively. Figure 4b depicts the nine solution regions as a function of riser direction azimuth λ and elevation δ angles, for the geometry of the main parachute suspension system used in the test cases presented in the next section. Only the boundary for case 0 is defined by means of an analytical constraint, as outlined earlier, whereas no direct simple method for determining the correct configuration of the bridles in tension is available for all the other ones, that is, given the position of

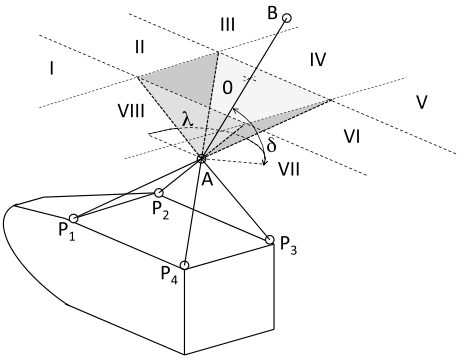

Fig. 3 Bridle pyramid and scheme for nonnominal cases.

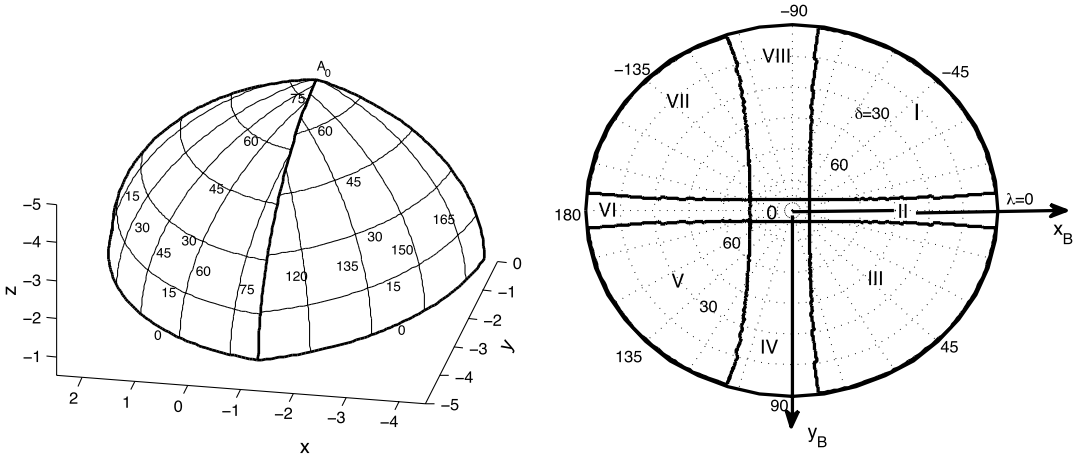

a) b)

Fig. 4 Position of riser attach point A for inextensible bridles as a function of riser azimuth and elevation: a) positions of A in $\mathcal{F}_B$ and b) solution regions.

Downloaded by Giorgio Guglieri on December 6, 2012 | http://arc.aiaa.org | DOI: 10.2514/1.C031788

B and a violation of the inequalities in Eq. (3), it is not possible to determine which one of the cases provides the correct position for A. Given the small number of cases present, a simple direct search is implemented. From the sign of the lateral coordinate of B, the possible cases are reduced from eight to five, that is, case 2 and 6, plus the three on the positive or negative portion of the y_V body axis.

All these five cases are solved and five tentative solutions for the position of A are obtained. To be acceptable, the distance of A from the attach points of the loose bridles for the considered case must be less than the length of the corresponding bridle. All of the tentative solutions but one usually result in a violation of the constraint on bridle length. Most of the time, the only admissible solution for A is then readily available simply by dropping the unfeasible ones. Occasionally, more than one of the tentative solutions are acceptable, in which case, the solution closest to B, which minimizes the tension in the riser and, as a consequence, the overall strain energy in the suspension system, is chosen. The tension in the taut bridle is equal to the tension in the riser, when only one bridle is in tension, whereas a simple vector decomposition provides the tension along the taut bridles, when one pair of bridles is loaded.

It is evident, at this point, that when a 3-D motion for the vehicle and parachute multibody system is to be investigated, the assumption of inextensible bridles results into a procedure that, although geometrically elegant, is quite cumbersome, especially if compared with the purely longitudinal case, where the direction of the risers immediately allows for the identification of the relevant case for the determination of the position of A and the corresponding tension in the suspension system. Nonetheless, once the set of possible cases is correctly identified, the implementation of the search algorithm described earlier results in an efficient procedure from the computational standpoint.

B. Fully Elastic System

When the bridles are assumed to be elastic, the position of the attach point A cannot be determined analytically, but a numerical scheme is necessary to derive simultaneously the position of A and the resulting tensions acting along the riser and the bridles. The vector $\boldsymbol{r}_{A_V} = (x_A, y_A, z_A)^T$ defines the (unknown) position of A in $\mathcal{F}_V$. The fixed position of bridle attach points on the vehicle P_i is represented as before by the vectors $\boldsymbol{r}_{P_i}$, $i = 1, 2, 3, 4$, whereas the position of the attach point B of the riser on the parachute side, seen in the vehicle's body frame, is given by

$$\boldsymbol{r}_{B_V} = \mathbb{T}_{VI}(\boldsymbol{r}_P - \boldsymbol{r}_I + \mathbb{T}_{IP}\boldsymbol{r}_{B_P})$$

To evaluate the coordinates of A at each time step, the suspension point A is assumed to be in a quasi-static equilibrium under the tensions developed by the four bridles and the riser. This means that Eq. (4) must hold, where the tension in the riser is evaluated in $\mathcal{F}_V$ as $\boldsymbol{f}_{r_V} = F_r(\boldsymbol{r}_{B_V} - \boldsymbol{r}_{A_V})/\ell_r$, with

$$\begin{aligned} F_r &= K_r(\ell_r - \ell_{r_0}) - C_r\dot{\ell}_r \quad \text{if } \ell_r > \ell_{r_0} \\ F_r &= 0 \qquad\qquad\qquad\qquad \text{if } \ell_r \le \ell_{r_0} \end{aligned}$$

with $\ell_r = \|\boldsymbol{r}_{B_V} - \boldsymbol{r}_{A_V}\|$, whereas the tension in the ith bridle is equal to $\boldsymbol{f}_{i_V} = F_i(\boldsymbol{r}_{P_i} - \boldsymbol{r}_{A_V})/\ell_i$, with

$$\begin{aligned} F_i &= K_{f/a}(\ell_i - \ell_{i_0}) \quad \text{if } \ell_i > \ell_{i_0} \\ F_i &= 0 \qquad\qquad\qquad\quad \text{if } \ell_i \le \ell_{i_0} \end{aligned}$$

with $\ell_i = \|\boldsymbol{r}_{P_i} - \boldsymbol{r}_{A_V}\|$. Note that, due to the lack of reliable information, damping in the suspension system is concentrated in the riser.

Equation (4) represents a system of three algebraic equations in three unknowns, namely the coordinates $(x_A, y_A, z_A)^T$ of A in $\mathcal{F}_V$, solved by means of a Newton–Raphson (N-R) method, in which the initial tentative value for the position of A is given by the coordinates $\boldsymbol{r}^*_{A_V} = (x^*_A, y^*_A, z^*_A)^T$ of A at the previous time step. Tolerance on the norm of the residual

$$\|\sum_{i=1}^{4} f_i\hat{\boldsymbol{\rho}}_i + \boldsymbol{f}_r\|$$

is set at $\varepsilon = 0.01$ N, equivalent to a relative accuracy of 10^{-6}, if vehicle's weight is used as the scaling parameter.

During the parachute opening phase, the distance between capsule and parachute due to snatch loads can be smaller than the unstretched length of bridles and riser. In this case, no tension is generated in both riser and bridles and the two bodies decouple instantaneously their dynamics. From a computational point of view, the N-R routine is tailored to recognize this feature (null Jacobian matrix), providing zero tension in all bridles and riser as output of the procedure. The position $\boldsymbol{r}_{A_V}$ becomes not relevant in this case, and the following step is initialized starting from the nominal position $\boldsymbol{r}^*_{A_V} = \boldsymbol{r}_{A_{0,V}}$.

The elements of the Jacobian matrix are evaluated by means of finite differences, whereas the value of $\dot{\ell}_r$ is evaluated by means of forward differences in time, starting from the solution at the previous time step. The procedure, which usually converges in a small number of iterations, between 5 and 10, to the desired accuracy. Although this numerical procedure needs to be performed four times at every step of the fourth-order Runge–Kutta algorithm used for the numerical simulation of the system, the computation time required remains a small fraction of the total time required for the integration step, thanks to the second-order convergence of the N-R method. This means that the use of this numerical procedure does not significantly affect the overall computation time necessary for performing a simulation, if compared with that necessary for performing the same simulation on the basis of the analytical method outline earlier for the case of inextensible bridles.

IV. Results

A. Sequence of Events

The nominal mission profile for the final reentry of the fictitious vehicle here considered is based on a sequence of two parachutes. A drogue slows the capsule from almost transonic speeds ($M = 0.85$) at an altitude of 20,000 m to low subsonic speeds ($M = 0.2$) at approximately 6000 m. The main parachute decelerates the capsule until touchdown, which takes place at a terminal speed of approximately 5 m/s with respect to the ground.

The nominal initial values for speed V, flight-path angle γ, altitude h, and angle of attack α reported in Table 2 define the nominal trajectory. Initial values for aerodynamic angles α and β and roll and pitch angles ϕ and θ are evaluated through a trim routine, which enforces equilibrium on external force and moments acting on the capsule. The trim condition depends on the location of the center of gravity (c.g.). In particular, nonzero values of roll and sideslip angles are required to balance lateral displacements of the c.g. from the vehicle symmetry plane.

Two multibody models presented in detail in Secs. II and III are considered for the vehicle and parachute assembly: model A, featuring a fully elastic model of the suspension system, with elastic bridles and riser, and model B, where the only elastic element is the riser and the bridles are assumed as inextensible. In both cases, the simulation is divided into four phases: 1) initialization and drogue ejection, lasting 1.5 s, during which the capsule is in freefall because no parachute is active; 2) deceleration from high to low subsonic regime, ending 150 s after drogue mortar firing, when drogue bridles are cut; 3) extraction of main chute bag by the drogue, which lasts 0.5 s, during which the vehicle is again in free fall; 4) main parachute deployment with a first reefing at 7% of its nominal area for 10 s, and final deceleration until touchdown, when the simulation is stopped after approximately 750 s from main chute release and 900 s from mortar firing.

The representation of parachute ejection and deployment is far from trivial because parachute release direction and its relative speed with respect to the vehicle play an important role in the determination of snatch loads and on peak values of capsule deceleration. In the nominal case, when a parachute is ejected (either drogue or main), it is assumed that the line connecting riser and parachute bag center of

Table 2 Nominal mission parameters and uncertainty distributions (U = uniform; G = Gaussian)

Variable	Symbol	Nominal value	Uncertainty	
			Type	Value
Initial conditions				
Mach number	M	0.85	U	0.1
Altitude	h	20 km	U	0.5 km
Angle of attack	α	65 deg	G	2.5 deg
Angle of sideslip	β	β_0 [a]	G	1 deg
Angular velocities	p, q, r	0 deg/s	G	0.2 deg/s
Flight-path angle	γ	−40 deg	G	2 deg
Attitude	ϕ, θ	ϕ_0, θ_0 [a]		
Drogue parachute				
Parachute bag release direction	λ, δ	λ_0, δ_0 [b]	G	2 deg
Relative speed with respect to capsule	ΔV	5 m/s	G	2 m/s
Main parachute				
Parachute bag release direction	λ, δ	λ_0, δ_0 [b]	G	2 deg
Relative speed with respect to capsule	ΔV	2 m/s	G	1 m/s

[a]Angles β_0, ϕ_0, and θ_0 are evaluated by means of vehicle moment trim.
[b]Angles λ_0, δ_0 are evaluated assuming parachute release parallel to wind direction.

Downloaded by Giorgio Guglieri on December 6, 2012 | http://arc.aiaa.org | DOI: 10.2514/1.C031788

gravity is parallel to the direction of the airstream impinging on the capsule. The release direction of the parachute bag is described by the azimuth λ angle in the x_V-y_V plane and elevation δ angle out of the plane, when at activation $\lambda \approx \beta - \pi$ and $\delta = \alpha$ (as β is always close to zero). Furthermore, as long as the drogue bag is extracted from the capsule by means of mortar firing, a relative velocity ΔV between bag and capsule is included in the model.

B. Effects of Uncertainties on the Nominal Solution

The nominal descent trajectory and the corresponding aerodynamic angles and deceleration profiles provide a reference behavior of the vehicle, parachute, and suspension lines in the final reentry phase. Uncertainties on the aerodynamic model and in the sequence of events in the previous phases of the reentry make the initial condition at the time of drogue mortar firing hardly predictable with great precision, so that the parachute-led reentry phase may start at an altitude, speed, and attitude slightly different from the nominal ones. Furthermore, the assumptions on parachute release angles and relative speed may provide results which differ from the actual system behavior.

The introduction of uncertainties on initial conditions for vehicle and parachute allows for a more reliable analysis of the expected behavior of the multibody system and suspension lines along the mission profile considered. A Monte Carlo analysis is performed perturbing the parameters listed in Table 2. Initial altitude and speed are perturbed with a uniform distribution, whereas the remaining perturbations follow a Gaussian distribution with a prescribed standard deviation σ.

For those parameters that are evaluated on the basis of vehicle trim condition, their value at trim is evaluated first, based on the perturbed system parameters. A perturbation is then added. In this way, the effect of deviations from trimmed flight condition at mortar firing is also included in the analysis. Only Euler angles are not perturbed because kinematic considerations relate univocally flight-path angle, angle of attack, and sideslip, with roll and pitch angles during the initial (almost) trimmed descent. The direction of the air impinging on the vehicle is assumed as the nominal release direction, which is perturbed by means of a Gaussian distribution, to account for the uncertainty in the position of the parachute bag at the time on inflation, when it is ejected in the highly turbulent wake downstream of the vehicle.

The effect of c.g. displacements from the symmetry plane is analyzed for model A only, to highlight the importance of a full-order three-dimensional simulation model on the evaluation of relevant performance parameters for the deceleration system. Almost identical results for trajectory, velocity, and attitude profiles are obtained for model B, featuring inextensible bridles, and are thus not reported in the results, for the sake of conciseness. Models A and B are finally compared, to evaluate if bridle elasticity affects deceleration profile and peak values of tensions in the suspension system. A total of four different configurations is thus considered: model A and B with nominal c.g., and model A with c.g. displaced to the left and the right of the symmetry plane. A total of 1000 runs are simulated for each configuration to generate a sufficiently large set of data for a reliable statistical analysis. The number was chosen by observing that the statistical properties of the sample is not affected by a further increase in the number of runs.

In the postprocessing phase, the evolution of mean value and standard deviation of the most important parameters and states with respect to time and Mach number is evaluated. For each run, the peak values of riser and bridles tension during the drogue opening, main reefed opening, and full deployment are identified to derive the statistical properties of maximum loads on the suspension lines.

1. *Trajectory for Model A with Centered Center of Gravity*

Figures 5–10 describe the behavior of the reference configuration, featuring a fully elastic suspension system (model A), when the c.g. lies in the longitudinal plane. Together with the nominal solution, the 3σ envelope evaluated from the results of the Monte Carlo analysis is reported, thus indicating the maximum expected deviation from the solution for the reference case. The trajectory in the Mach-altitude plane is plotted in Fig. 5, where the time line of events is also reported. It is evident from this plot that, when the drogue or the main parachute are deployed, speed is reduced abruptly first, with a limited altitude loss. After this transient (e.g., the deceleration from $M \approx 0.2$–0.03 at main chute deployment), an equilibrium between vehicle

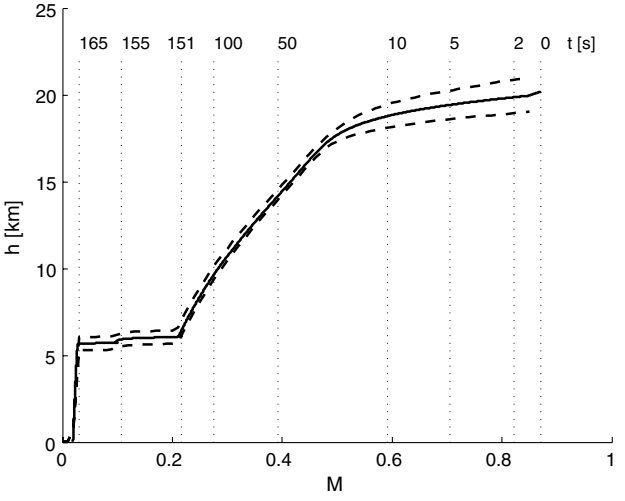

Fig. 5 Altitude vs Mach number for model A (solid line, nominal case; dashed line, 3σ envelope).

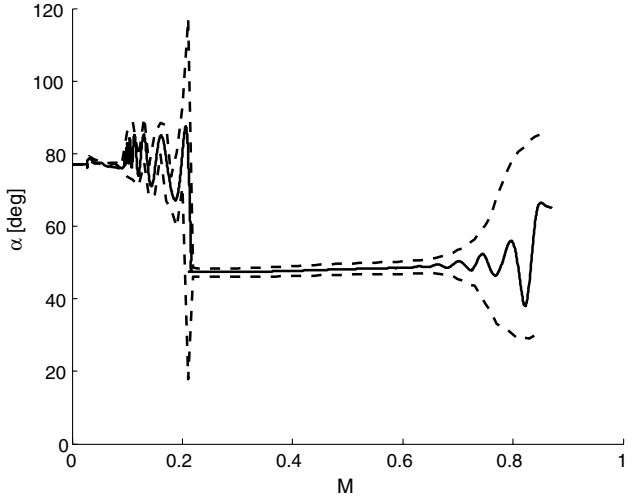

Fig. 6 Angle of attack vs Mach number for model A (solid line, nominal case; dashed line, 3σ envelope).

Downloaded by Giorgio Guglieri on December 6, 2012 | http://arc.aiaa.org | DOI: 10.2514/1.C031788

weight and parachute drag (with a small contribution from the capsule) is reached. In this steady-state descent, speed is slowly reduced simply because of the higher density of the atmosphere at lower altitude, which in turn increases parachute drag.

The attitude of capsule and parachute during steady-state descent, strongly dependent on the geometry of the suspension lines (in particular on the length of the bridles), is reached in general for an angle of attack different with respect to that at the time of mortar firing. This difference in vehicle attitude during the free-fall phases and steady-state descent after drogue/parachute inflation causes oscillations during the parachute deployment phase, clearly visible in Fig. 6 for the nominal solution. In the presence of uncertainties, the amplitude of these oscillations may vary significantly, and it is accompanied by variations in the total deceleration (expressed in terms of time derivative of the velocity magnitude) as large as 40% for the peak value of $\mathrm{d}V/\mathrm{d}t$ at drogue deployment and 20%, when the main parachute is deployed (Fig. 7). In the latter figure, it is noteworthy to observe that the effects of uncertainties rapidly drops. This is particularly visible at drogue deployment, which is more affected by the uncertainty on initial conditions: After only 5 s from mortar firing (i.e., $M < 0.7$), the amplitude of the 3σ envelope, which accounts for 99.7% of the test cases, is significantly reduced and remains small for the whole remaining portion of the deceleration. A second uncertainty peak is visible at main parachute deployment ($t \approx 151$ s and $M < 0.2$).

During drogue deployment and staged inflation of the main parachute, peak values for tensions in the suspension systems are

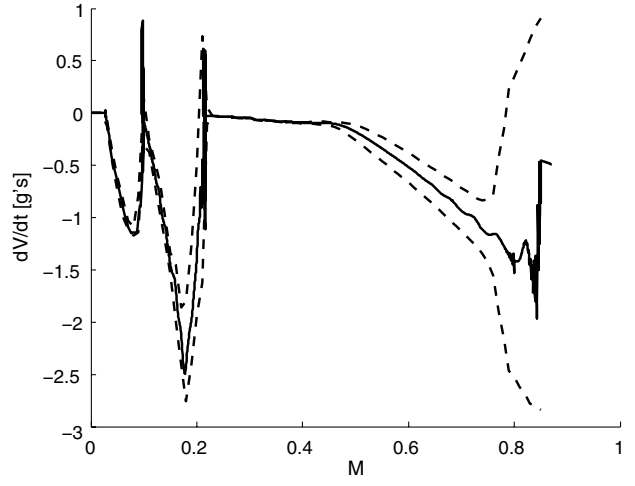

Fig. 7 Deceleration vs Mach number for model A (solid line, nominal case; dashed line, 3σ envelope).

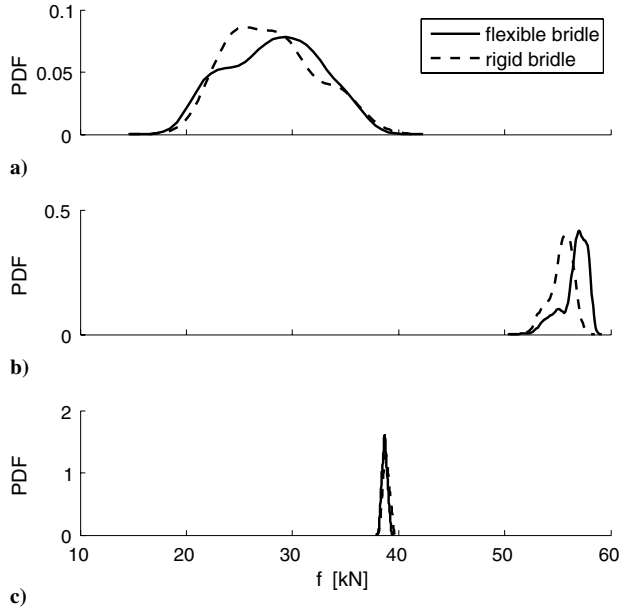

Fig. 8 PDF of peak values for a) riser tension during drogue deployment, b) main chute first reefing stage, c) and main chute full inflation for models A (solid line) and B (dashed line).

reached (snatch loads). A reliable estimate of this peaks for every possible nonnominal operating condition is of paramount importance for correctly sizing bridles and riser. For this reason, a statistical analysis of the maximum tension reached in each element of the suspension system during the final deceleration phase is performed for the 1000 runs of the Monte Carlo analysis. Peak values are reached during drogue opening (Fig. 8a), first reefing stage of the main parachute (Fig. 8b), and main parachute full deployment (Fig. 8b). The probability density functions (PDFs) of maximum riser and bridle tension during these phases are reported in Figs. 8 (solid line) and 9, respectively.

The PDFs of riser and bridle tension during drogue deployment show a wide distribution because the effects of the uncertainty introduced in the initial conditions are significant. On the converse, the initial conditions at main chute deployment depend on the descent condition acquired under the decelerating action of the

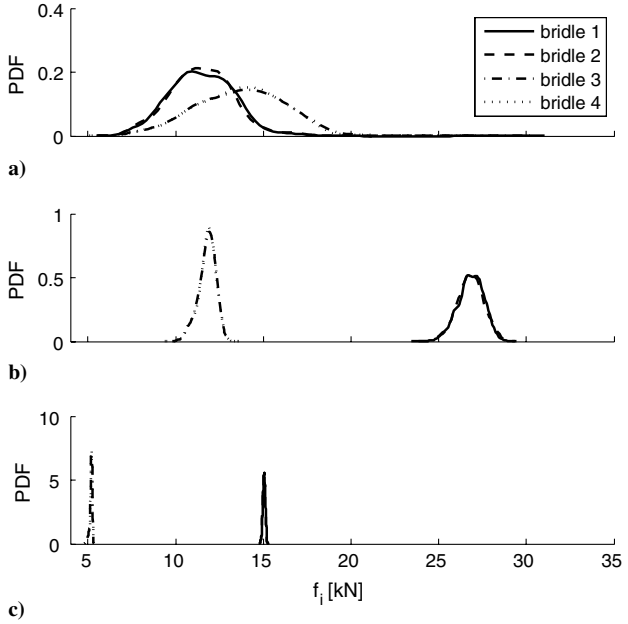

Fig. 9 PDF of peak values for tension in a) the bridles during drogue deployment, b) main chute first reefing stage, and c) main chute full inflation for model A.

Downloaded by Giorgio Guglieri on December 6, 2012 | http://arc.aiaa.org | DOI: 10.2514/1.C031788

drogue, for the first reefing stage, and on the descent condition with a reefed main, when the main chute is fully inflated. This makes the initial conditions for the second and third phases vary in a much narrower range. A worst case of 40 kN in riser tension and 20 kN in bridle tension are encountered, at drogue deployment, whereas loads are higher on riser and bridles of the main parachute during the deployment of the first reefing stage, being close to 60 and 30 kN in the worst cases. Also note from Fig. 9 that aft bridles are more loaded during drogue release (Fig. 9a), whereas forward bridles are expected to withstand higher loads during the first reefing stage of the main chute (Fig. 9b). Peaks during full main inflation are significantly lower, and the suspension system of the main chute should be sized against the snatch load during the first reefing stage. Note that, if the c.g. lies on the longitudinal plane, left and right pairs of bridles are expected to sustain (statistically) the same loads.

Together with peak values for deceleration and tension in the suspension system, the Monte Carlo analysis allows for the determination of the sensitivity of the landing spot with respect to the uncertainties introduced in the model. Note that this is not the actual expected landing footprint, which is strongly influenced by winds and atmospheric turbulence, not considered in the present model. Nonetheless, the effect of uncertainties on the landing (or splashdown) site is evaluated quantitatively. When the c.g. lies in the longitudinal plane and no lateral-longitudinal coupling terms are included in the inertia tensor, the cross-range displacement at touchdown is mainly determined by the perturbation on the initial conditions and, in particular, by the azimuth angle of the parachute bag at canopy opening. Figure 10 shows that the landing area is centered around a downrange of approximately 7 km, with a standard deviation σ of approximately 0.5 km in both the longitudinal (downrange) and lateral (cross-range) directions.

Summarizing the analysis of the results obtained from the 1000 test cases run for the Monte Carlo simulation, one notes that uncertainties on initial values of riser azimuth and elevation do not affect significantly peak values of deceleration $\dot{V}$ and tensions in the suspension system. Conversely, peak values for tensions exhibit a pronounced sensitivity to the initial values of parachute bag relative speed after mortar firing, $v_r = \|\boldsymbol{v}_P - \boldsymbol{v}_V\|$ at time zero, increasing almost linearly with v_r. The correlation of v_r with peak values of the deceleration $\dot{V}_{\max}$ is poorer. Also, the initial value of the angle of attack affects $\dot{V}_{\max}$ and peak values for tension in the suspension lines, although to a lesser extent, whereas uncertainties on β in the range considered induce variations hardly noticeable. Quite obviously, $\dot{V}_{\max}$ is correlated to the initial value of the Mach number, increasing almost linearly with it.

Finally, one should note that the uncertainty on initial conditions affects the dispersion of data only for the initial phase of the deceleration process, at drogue deployment. The 3σ envelope becomes rapidly narrower when the variation of relevant parameters is reported as a function of Mach number. The amplitude of the 3σ envelope increases again at parachute deployment, but remaining less wide than at the beginning of the final deceleration phase.

2. *Effect of Center of Gravity Position*

In the reference case, the capsule c.g. lies in the longitudinal plane, but its actual position is usually not known exactly, so that the sensitivity of the results to c.g. displacements from its nominal location needs to be evaluated. The major effect of longitudinal shift of the c.g. is a variation of the trim angle of attack of vehicle during free-fall phases and of the vehicle-parachute system during decelerated phases. As a consequence, also the descent angle is affected, because of the different aerodynamic efficiency when flying at a nonnominal trim incidence. These results are not reported here because tensions in the suspension system are only marginally affected and the landing footprint simply moves forward in those cases when γ becomes less negative, or backward, if the descent angle is increased. The cross range is not affected at all and the trajectory remains mostly a longitudinal one. Most of the performances are correctly evaluated by means of the (significantly simpler) purely longitudinal model with rigid bridles (also not reported here, for the sake of conciseness).

On the converse, a lateral displacement of the c.g. causes a more significant coupling between longitudinal- and lateral-directional dynamics. The moment arm of left and right pairs of bridles is changed, so that the vehicle at trim is characterized by a nonzero value of sideslip and roll angles β and ϕ, and the trajectory of parachute and vehicle bends in one direction, so that a large turn is performed, with the yaw angle increasing almost linearly with time (Fig. 11). At low speed, after main parachute inflation, the trajectory becomes close to vertical, but a significant displacement on one side of the initial trajectory plane is achieved during the previous, uncontrolled phase.

Note that a 3-D model is required for evaluating the effects of lateral c.g. displacements, but when vehicle lateral-directional dynamics is open-loop stable, as in the present case, in the whole considered speed range, a linear variation of aerodynamic coefficients with angular velocity components and sideslip angles like that presented in Sec. II is sufficient. This is proven by the results reported in Fig. 12, where the variation of airspeed, angle of attack, and sideslip angle with time is reported. Also during drogue and parachute deployment phases at $t = 1.5$ s and $t \approx 150$ s, the sideslip angle remains smaller than 2 deg, in spite of the large variations of airspeed and angle of attack.

Two sets of tests are performed by shifting the vehicle c.g. 5 mm to the right and to the left of the longitudinal plane. This is done with the objective of validating the model, which must provide symmetric dispersions of the results with respect to the nominal trajectory plane. Longitudinal- and lateral-directional dynamics of the two-body system become coupled. Sensitivity of the landing spot with respect

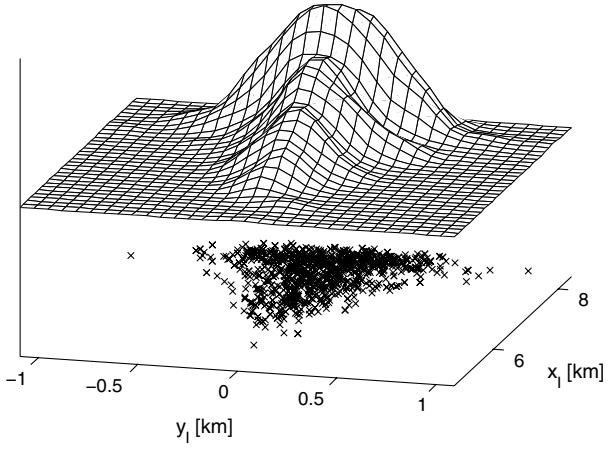

Fig. 10 Landing footprint PDF.

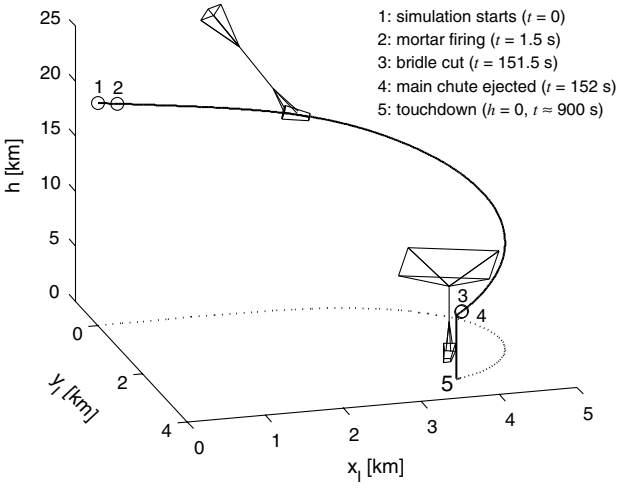

Fig. 11 Trajectory with c.g. displaced from longitudinal plane.

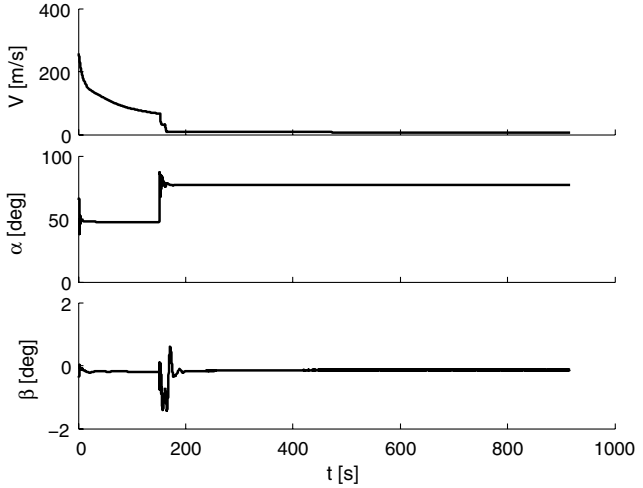

Fig. 12 Nominal time evolution of speed, angle of attack, and sideslip for a spacecraft with displaced c.g.

to a displaced lateral c.g. location (for a value of ± 5 mm) is shown in Fig. 13 for 1000 Monte Carlo runs, where the same 14 parameters are perturbed at simulation start. The landing footprint with displaced c.g. is characterized by a higher cross range, achieved during the initial turn when the drogue is deployed and a reduced downrange. The 1σ landing footprint is transformed from an almost triangular shape to a bean-like shape, disjoint from that obtained for the almost purely longitudinal solutions with the nominal c.g. position. The uncertainties introduced in the Monte Carlo analysis perturb the nominal solution, but the most important features of the trajectory are dominated by the c.g. location, as demonstrated by the small dispersion area and the narrow peak around the nominal solution with displaced c.g. and zero uncertainties, placed almost exactly at the maximum of the two-dimensional PDF in the *x*-*y* plane.

As a final observation, the location of vehicle c.g. has a limited impact on peak values of vehicle deceleration and tension in the suspension lines. A minor difference is present only when the first reefing stage of the main chute is deployed. At this point, the 3σ envelope for the acceleration is increased by 15% with respect to the results obtained for the nominal c.g. position on the longitudinal plane. This is coupled with wider oscillations induced by the direction of parachute bag at release, which is displaced sideways because of a more pronounced banked and sideslipped attitude and the slow spin rate around the vertical axis. The effects of this higher deceleration on peak values of riser and bridle tension is relatively small, but not negligible. On the converse, differences are marginal in all the remaining portions of the descent. This proves that a 2-D analysis is sufficient for preliminary sizing purposes of the suspension system, whereas a more detailed 3-D model is necessary for a more accurate determination of peak loads and the identification of the landing footprints, the latter significantly affected by lateral c.g. displacement.

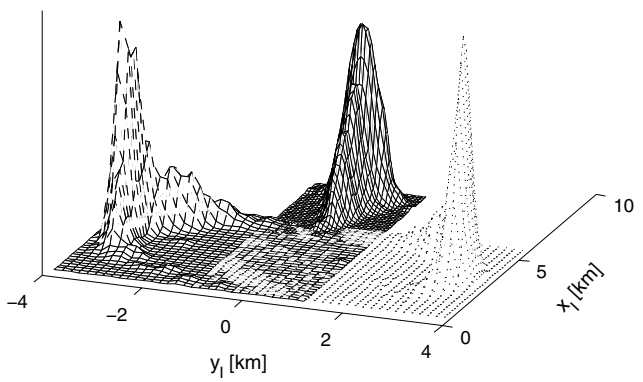

Fig. 13 Dispersion of the landing spot for nominal c.g. position (solid line), left (dashed line), and right (dotted line) c.g. displacements.

C. Inextensible vs Elastic Bridles

In all the previous cases, model A was considered, which features a fully elastic bridle model that requires a numerical iterative scheme for the determination of the position of the riser attach point *A* on the vehicle's side and the corresponding tension in the suspension lines. As outlined earlier, an analytical solution for the determination of the position of *A* and the resulting bridle tension is available. As long as an assumption of rigid bridles is common practice, an analysis of the effects of bridle model on the accuracy of the solution and computational burden is of interest.

1. Accuracy of the Results

The trajectories obtained by means of flexible and inextensible bridles approach almost overlap exactly, and for this reason they are not presented. Peak values of tension in the riser are distributed around values slightly lower for the inextensible bridle case during drogue opening and first reefing stage of the main chute (Figs. 8a and 8b, respectively). Note that worst case scenarios (which determine the requirement for sizing the suspension lines) present tensions that are almost exactly equal.

Figure 14 shows the PDF for the peaks in bridle tension during the three deployment stages. The only significant changes are visible during the first stage of reefing of the main parachute (Fig. 8b), when the loads evaluated for the aft bridles are higher in the inextensible case. On the converse, during final inflation of the main chute (Fig. 8c), loads on forward are approximately 10% higher than those estimated for the full elastic case, whereas those on the aft bridles are 10% lower. Yet the order of magnitude necessary for sizing the suspension lines is identified with sufficient precision even when the inextensible bridle model is adopted.

An even simpler model is available, if one assumes that the position of the attach point *A* is not affected by the direction of riser tension. This means that point *A* is assumed to lie always in its nominal position A_0, geometrically determined for the considered values of bridles' length. If this simplifying assumption is adopted, no iterative procedure (model A) nor search scheme (model B) are necessary. At the same time, two major problems arise. First of all, the variation of the position of *A* significantly affects the moment arm with which riser tension acts on the vehicle. This means that, when the riser swings laterally and/or longitudinally, higher moments are transmitted to the vehicle and the correct identification of stability for the two-body system may be hindered. At the same time, it becomes

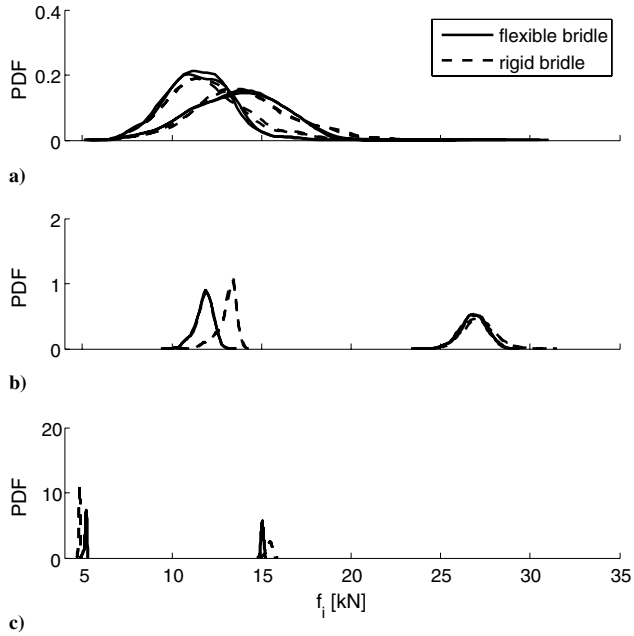

Fig. 14 PDF of peak values of tension in a) the bridles during drogue deployment, b) main chute first reefing stage, and c) main chute full inflation for models A (solid line) and B (dashed line).

Downloaded by Giorgio Guglieri on December 6, 2012 | http://arc.aiaa.org | DOI: 10.2514/1.C031788

impossible to evaluate tension in the bridles, as some of them should provide a compression force not physically admissible.

2. Computational Burden

From a computational point of view, the routine that evaluates suspension line loads based on inextensible bridles is twice as fast as the one based on flexible bridles. Despite this cost advantage, the time saved in a complete simulation is only marginal due to the fact that the computational cost for the evaluation of suspension lines load is only 4.1 and 1.9% of the total simulation cost for flexible and inextensible bridles, respectively. Given a computation time of 16.38 and 16.01 s on a 2.2 GHz CPU for an average simulation from 20,000 m to touchdown, the time saved with the inextensible bridles approach is approximately 0.4 s. Such a figure is not significant, also if time-consuming Monte Carlo runs are to be performed and, as a consequence, the fully elastic system provides a numerically reliable way of simulating the whole suspension lines. Note that this consideration applies also to the simplest model, when point A is assumed always coincident with A_0 and 0.8 s out of 16 s are saved, that is, only 5% of the total CPU time.

V. Conclusions

A multibody analysis of a system formed by an entry vehicle and a parachute is presented. The nominal mission profile considered for the reference reentry vehicle is based on the deployment of a sequence of two parachutes, a high-speed drogue, and a main decelerator. Two different models of the suspension system made of four bridles and a riser connecting the vehicle to the canopy suspension lines are implemented and tested. Monte Carlo analyses based on groups of 1000 runs are performed to account for uncertainties on initial conditions and system parameters for four different configurations, including lateral displacement of vehicle center of mass from the longitudinal plane.

The results highlight that the flexibility of the bridles has a limited effect on payload attitude dynamics and estimate of tension in the suspension lines. Changes in maximum deceleration and peak loads are within 10% of the nominal value, whereas the trajectory is almost unaffected. The lateral position of vehicle center of gravity has a major effect (as expected) on the trajectory, causing a significant increment of the cross range, at the expense of a reduced downrange. From a computational point of view, the routine that evaluates suspension line loads with inextensible bridles is twice as fast as the full-flexible approach. Nevertheless, because both routines require only a small fraction of the total simulation time (dominated by vehicle and parachute aerodynamic models), the computational cost advantage is limited.

Downloaded by Giorgio Guglieri on December 6, 2012 | http://arc.aiaa.org | DOI: 10.2514/1.C031788

Acknowledgments

Financial support from Thales Alenia Space through contract T386-AS-2010-01 is acknowledged. The authors express their gratitude to Alessandro Palmas, for his support in the development of the vehicle-parachute mathematical model.

References

[1] Portigliotti, S., Paulat, J. C., and Rives, J., "ARD Descent and Recovery Subsystem Dynamics and Trajectory Flight Data Evaluation," *1st AAAF International Symposium on Atmospheric Reentry Vehicles and Systems*, AAAF Paper 18.4, Paris, France, 1999, pp. 1–10.

[2] Portigliotti, S., "Parachute Flight Dynamics Modeling and Simulation: Code Validation Through ARD Post-Flight Analysis," *2nd AAAF International Symposium on Atmospheric Reentry Vehicles and Systems*, AAAF Paper 8.2, Paris, France, 2001, pp. 1–10.

[3] De Giorgis, M., Borriello, G., Allasio, A., Vavala, R., Laveugle, T., and Cosentino, O., "Atmospheric Reentry Demonstrator Balloon Flight Test," *Journal of Spacecraft and Rockets*, Vol. 36, No. 4, 1999, pp. 507–510. doi:10.2514/3.27192

[4] Moseley, W. C., Moore, R. H., and Hughes, J. E., "Stability Characteristics of the Apollo Command Module," NASA Manned Spacecraft Center, NASA TN-D-3890, Houston, TX, 1967.

[5] Guglieri, G., and Quagliotti, F. B., "Low Speed Dynamic Tests on a Capsule Configuration," *Aerospace Science and Technology*, Vol. 4, No. 6, 2000, pp. 383–390. doi:10.1016/S1270-9638(00)01066-X

[6] Guglieri, G., and Quagliotti, F. B., "Validation of a Simulation Model for a Planetary Entry Capsule," *Journal of Aircraft*, Vol. 40, No. 1, 2003, pp. 127–136. doi:10.2514/2.3067

[7] Tumino, G., "The IXV Project: The European In-Flight Experimentation for Future Space Transportation Systems and Technologies," *58th International Astronautical Congress*, IAC-07-D2.6.02, 2007.

[8] Tumino, G., "The IXV Project: The ESA Reenty System and Technologies Demonstrator Paving the Way to European Autonomous Space Transportation and Exploration Endeavours," *59th International Astronautical Congress*, IAC-08-D2.6.1, 2008.

[9] Desai, P. N., Braun, R. D., Powell, R. W., Engelund, W. C., and Tartabini, P. V., "Six-Degree-of-Freedom Entry Dispersion Analysis for the METEOR Recovery Module," *Journal of Spacecraft and Rockets*, Vol. 34, No. 3, 1997, pp. 334–340. doi:10.2514/2.3213

[10] Braun, R. D., Powell, R. W., Engelund, W. C., Gnoffo, P. A., Weilmuenster, K. J., and Mitcheltree, R. A., "Mars Pathfinder Mission Six-Degree-of-Freedom Entry Analysis," *Journal of Spacecraft and Rockets*, Vol. 32, No. 6, 1995, pp. 993–1000. doi:10.2514/3.26720

[11] Desai, P. N., and Knocke, P. C., "Mars Exploration Rovers Entry, Descent, and Landing Trajectory Analysis," *Journal of the Astronautical Sciences*, Vol. 55, No. 3, 2007, pp. 311–323. doi:10.1007/BF03256527

[12] Spencer, D. A., Blanchard, R. C., Braun, R. D., Kallemeyn, P. H., and Thurman, S. W., "Mars Pathfinder Entry, Descent and Landing Reconstruction," *Journal of Spacecraft and Rockets*, Vol. 36, No. 3, 1999, pp. 357–366. doi:10.2514/2.3478

[13] Desai, P. N., Mitcheltree, R. A., and Cheatwood, F. M., "Entry Dispersion Analysis for the Stardust Comet Sample Return Capsule," *AIAA GNC, AFM, and MST Conference and Exhibit*, AIAA Paper 97-3812, 1997.

[14] Atkinson, D. H., Kazeminejad, B., Gaborit, V., Ferri, F., and Lebreton, J. P., "Huygens Probe Entry and Descent Trajectory Analysis and Reconstruction Techniques," *Planetary and Space Science*, Vol. 53, No. 5, 2005, pp. 586–593. doi:10.1016/j.pss.2004.11.005

[15] Baillion, M., "Blunt Bodies Dynamic Derivatives," AGARD R-808, 1997.

[16] Ericsson, L. E., and Reding, J. P., "Re-Entry Capsule Dynamics," *Journal of Spacecraft and Rockets*, Vol. 8, No. 6, 1971, pp. 579–586. doi:10.2514/3.59696

[17] "Deployable Aerodynamic Deceleration Systems," NASA Langley Research Center, NASA-SP-8066, 1971.

[18] Knacke, T. W., "The Apollo Parachute Landing System," *2nd AIAA Aerodynamic Decelerator Systems Technology Conference*, AIAA, Washington, D.C., 1968, pp. 1–28.

[19] Cockrell, D. J., and Young, A. D., "The Aerodynamics of Parachutes," AGARD AG-295, 1987.

[20] Maydew, R. C., and Peterson, C. W., "Design and Testing of High Performance Parachutes," AGARD AG-319, 1991.

[21] Cruz, J. R., and Lingard, S., "Aerodynamic Decelerators for Planetary Exploration: Past, Present, and Future," *AIAA Guidance, Navigation, and Control Conference and Exhibit*, AIAA, Reston, VA, 2006;see also AIAA Paper 2006-6792.

[22] Hume, R. G., "A Two Dimensional Mathematical Model of a Parachute in Steady Descent," Aeronautical Research Council, CP 1260, 1973.

[23] Neustadt, M., Ericksen, R. E., Guiteras, J. J., and Larrivee, J. A., "A Parachute Recovery System Dynamic Analysis," *Journal of Spacecraft and Rockets*, Vol. 4, No. 3, 1967, pp. 321–326. doi:10.2514/3.28860

[24] White, F. M., Rhode Island, U., Kingston, R. I., and Wolf, D. F., "A Theory of Three-Dimensional Parachute Dynamic Stability," *Journal of Aircraft*, Vol. 5, No. 1, 1968, pp. 86–92. doi:10.2514/3.43912

[25] Wolf, D. F., "Dynamic Stability of a Nonrigid Parachute and Payload System," *Journal of Aircraft*, Vol. 8, No. 8, 1971, pp. 603–609. doi:10.2514/3.59145

[26] Doherr, K. F., and Schilling, H., "Nine Degree-of-Freedom Simulation of Rotating Parachute Systems," *Journal of Aircraft*, Vol. 29, No. 5, 1992, pp. 774–781. doi:10.2514/3.46245

[27] Tory, C., and Ayres, R., "Computer Model of a Fully Deployed

Parachute," *Journal of Aircraft*, Vol. 14, No. 7, 1977, pp. 675–679. doi:10.2514/3.58839

[28] Eaton, J. A., "Added Masses and the Dynamic Stability of Parachutes," *Journal of Aircraft*, Vol. 19, No. 5, 1982, pp. 414–416. doi:10.2514/3.44766

[29] Eaton, J. A., "Added Fluid Mass and the Equations of Motion of a Parachute," *Aeronautical Quarterly*, Vol. 34, No. 8, Jan. 1984, pp. 226–242.

[30] Cuthbert, P. A., "A Software Simulation of Cargo Drop Test," *17th AIAA Aerodynamic Decelerator Systems Technology Conference*, AIAA Paper 2003-2132, 2003.

[31] Cuthbert, P. A., and Desabrais, K. J., "Validation of a Cargo Airdrop Simulator," *17th AIAA Aerodynamic Decelerator Systems Technology Conference*, AIAA Paper 2003-2133, 2003.

[32] Etkin, B., *Dynamics of Atmospheric Flight*, Wiley, New York, 1972, pp. 104–120.

[33] Cockrell, D. J., Eaton, J. A., and Morgan, C. J., "Longitudinal Oscillation Damping for Fully-inflated Parachute Canopies," *6th AIAA Aerodynamic Decelerator and Balloon Technology Conference*, AIAA, New York, 1979, pp. 1–5;see also AIAA Paper 79-0459.

Downloaded by Giorgio Guglieri on December 6, 2012 | http://arc.aiaa.org | DOI: 10.2514/1.C031788